UNIVERSITÄT PADERBORN
Die Universität der Informationsgesellschaft

Fakultät für Elektrotechnik, Informatik und Mathematik
Arbeitsgruppe Quanteninformatik

Classical Simulation of Quantum Circuits with Restricted Boltzmann Machines

Master's Thesis

in Partial Fulfillment of the Requirements for the Degree of

Master of Science

by
Jannes Stubbemann

submitted to:
Jun. Prof. Dr. Sevag Gharibian
and
Prof. Dr. Eyke Hüllermeier

Paderborn, August 6, 2020

Declaration

(Translation from German)

I hereby declare that I prepared this thesis entirely on my own and have not used outside sources without declaration in the text. Any concepts or quotations applicable to these sources are clearly attributed to them. This thesis has not been submitted in the same or substantially similar version, not even in part, to any other authority for grading and has not been published elsewhere.

Original Declaration Text in German:

Erklärung

Ich versichere, dass ich die Arbeit ohne fremde Hilfe und ohne Benutzung anderer als der angegebenen Quellen angefertigt habe und dass die Arbeit in gleicher oder ähnlicher Form noch keiner anderen Prüfungsbehörde vorgelegen hat und von dieser als Teil einer Prüfungsleistung angenommen worden ist. Alle Ausführungen, die wörtlich oder sinngemäß übernommen worden sind, sind als solche gekennzeichnet.

City, Date

Signature

Contents

1 Nomenclature and Notations

This chapter introduces mathematical notations and expressions used throughout this study. Its focus is on linear algebra, the mathematical foundation of *quantum mechanics*. It is thought as a lookup reference for the following chapters.

Vectors are represented in the *Bra-ket* notation. *Ket*-vectors $|\psi\rangle$ denote column vectors:

$$|\psi\rangle = \begin{pmatrix} \alpha \\ \beta \end{pmatrix}. \tag{1.1}$$

The *bra* $\langle\psi|$ of a vector $|\psi\rangle$ is its hermitian conjugate, $\langle\psi| = |\psi\rangle^\dagger$. It is the transpose of the vector with complex-conjugated entries. For the ket vector $|\psi\rangle$ above, the corresponding bra-vector would be:

$$\langle\psi| = \begin{pmatrix} \alpha^* & \beta^* \end{pmatrix}, \tag{1.2}$$

where the complex-conjugate of some complex number $\alpha = a + bi$ is defined as $\alpha^* = a - bi$. Using this notation, the *inner product* of two vectors $|\psi\rangle$ and $|\phi\rangle$ can be written as:

$$\langle\psi \,|\, \phi\rangle = \sum_j \psi_j^* \phi_j. \tag{1.3}$$

The *outer product* $|\psi\rangle \langle\phi|$ defines the matrix A with entries a_{ij} given by:

$$a_{ij} = \psi_i \phi_j^*. \tag{1.4}$$

The class of matrices of special interest in quantum computing are *unitary* matrices. A complex-valued square matrix U is unitary if:

$$UU^\dagger = U^\dagger U = I. \tag{1.5}$$

Unitary matrices are norm preserving and thus represent rotations in the vector space. The *tensor product* $\cdot \otimes \cdot$ of two matrices $A = \begin{pmatrix} a_{11} & a_{12} \\ a_{21} & a_{22} \end{pmatrix}$ and $B = \begin{pmatrix} b_{11} & b_{12} \\ b_{21} & b_2 2 \end{pmatrix}$ is defined as:

$$A \otimes B = \begin{pmatrix} a_{11}B & a_{12}B \\ a_{21}B & a_{22}B \end{pmatrix} \tag{1.6}$$

$$= \begin{pmatrix} a_{11}b_{11} & a_{11}b_{12} & a_{12}b_{11} & a_{12}b_{12} \\ a_{11}b_{21} & a_{11}b_{22} & a_{12}b_{21} & a_{12}b_{22} \\ a_{21}b_{11} & a_{21}b_{12} & a_{22}b_{11} & a_{22}b_{12} \\ a_{21}b_{21} & a_{21}b_{22} & a_{22}b_{21} & a_{22}b_{22} \end{pmatrix}. \tag{1.7}$$

The dimensions of the tensor product of two matrices with dimensions $n_A \times m_A$ and $n_B \times m_B$ is $n_A n_B \times m_A m_B$. The tensor product for vectors is defined accordingly. The *Kroenecker Delta* δ_{ij} sometimes occurs in quantum physics. It is defined as:

$$\delta_{ij} = \begin{cases} 1, & \text{if } i = j, \\ 0, & \text{if } i \neq j. \end{cases} . \tag{1.8}$$

and by that defines the dot product of two vectors $|\psi_i\rangle$ and $|\psi_j\rangle$ from a set of orthonormal vectors.

2 Quantum Computing

This chapter gives an introduction to the field of *Quantum Computation*. It covers the basics of qubits, quantum gates and circuits, and gives an overview of quantum complexity classes. The chapter is based on [27], which offers a profound introduction into the field.

2.1 Qubits

While classical computers harness classical physical phenomena like electrical current to perform calculations, quantum computers harness *quantum mechanical* effects. The simplest quantum mechanical system is a quantum bit, or *qubit* for short. It is the fundamental building block of a quantum computer.

Mathematically, a qubit is a two-dimensional complex-valued unit vector, also called the *state vector* or *wave function*:

$$|\psi\rangle = \begin{pmatrix} \alpha \\ \beta \end{pmatrix} \tag{2.1}$$

with *amplitudes* $\alpha, \beta \in \mathbb{C}$ and $|\alpha|^2 + |\beta|^2 = 1$. Rewriting $|\psi\rangle$ as

$$|\psi\rangle = e^{i\gamma} \left(\cos\frac{\theta}{2} |0\rangle + e^{i\rho} \sin\frac{\theta}{2} |1\rangle \right) \tag{2.2}$$

with $\theta, \rho, \gamma \in \mathbb{R}$ allows an intuitive interpration of a qubit as a point on the surface of the three-dimensional unit sphere, called the *Bloch Sphere*, which is visualized in figure **??**. The factor $e^{i\gamma}$ in front is called a *global phase* and can be ignored:

$$|\psi\rangle = \cos\frac{\theta}{2} |0\rangle + e^{i\rho} \sin\frac{\theta}{2} |1\rangle . \tag{2.3}$$

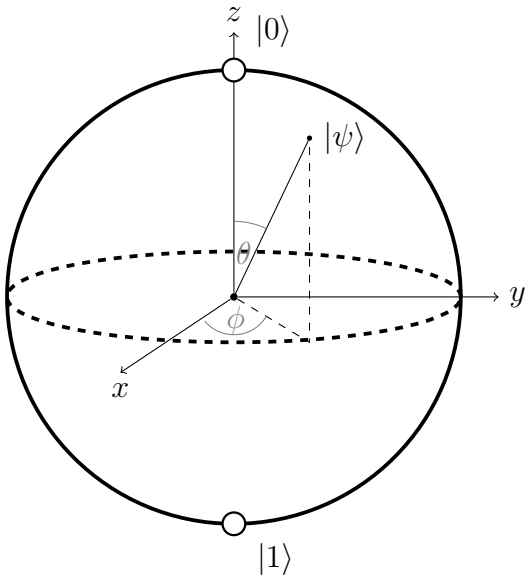

Figure 2.1: Bloch Sphere representation of a qubit state $|\psi\rangle$. $|\psi\rangle$ points to an arbitrary direction on the three dimensional unit sphere.

The states on the north and south pole of the Bloch Sphere are called the *computational basis states*, defined as:

$$|0\rangle = \begin{pmatrix} 1 \\ 0 \end{pmatrix} \tag{2.4}$$

and

$$|1\rangle = \begin{pmatrix} 0 \\ 1 \end{pmatrix}. \tag{2.5}$$

These states correspond to the classical states 0 and 1 of a classical bit. Thus, another way of writing the wave function of a qubit, which is also the most practical one for quantum computation, is a linear combination of the two computational basis states:

$$|\psi\rangle = \alpha \cdot |0\rangle + \beta \cdot |1\rangle. \tag{2.6}$$

A qubit whose amplitudes α and β are both non-zero is in a so-called *superposition* of the two computational basis states. A qubit in a superposition can be interpreted as being in both states $|0\rangle$ and $|1\rangle$ at the same time. This property is one of the underlying reasons why the classical simulation of quantum systems is computationally so hard, and it is one of the sources of the potential computational power of quantum computers. Nevertheless, it is not possible to read the values of the amplitudes α and β directly.

The qubit can only be in a superposition as long as it is completely isolated from its environment. Such a state is called a *coherent* state. As soon as the qubit

interacts with its environment, as it is necessary to read its value, it collapses randomly into one of the two computational basis states. All the information that was stored in the amplitudes gets lost in this process.

In a quantum computer, the qubits are in a coherent state, and potentially in a superposition, during the computation. At the end of the computation, a so-called *projective measurement* is performed to read the states of the individual qubits. A projective measurement is given by *operators* $\mathbf{M} = \{M_i\}$, in this case $M_0 = |0\rangle\langle 0|$ and $M_1 = |1\rangle\langle 1|$. The probabilities $p(0)$ and $p(1)$ of observing a qubit in the $|0\rangle$ or $|1\rangle$ state are then defined by the amplitudes:

$$\begin{aligned} p(0) &= \langle\psi| M_0^\dagger M_0 |\psi\rangle && (2.7)\\ &= \langle\psi| M_0 |\psi\rangle && (2.8)\\ &= \alpha \langle 0 \,|\, 0\rangle \langle 0| \alpha |0\rangle + \beta \langle 1 \,|\, 0\rangle \langle 0| \beta |1\rangle && (2.9)\\ &= \alpha^2 \langle 0 \,|\, 0\rangle \langle 0 \,|\, 0\rangle + \beta^2 \langle 1 \,|\, 0\rangle \langle 0 \,|\, 1\rangle && (2.10)\\ &= \alpha^2 && (2.11) \end{aligned}$$

and

$$\begin{aligned} p(1) &= \langle\psi| M_1^\dagger M_1 |\psi\rangle && (2.12)\\ &= \langle\psi| M_1 |\psi\rangle && (2.13)\\ &= \alpha \langle 0 \,|\, 1\rangle \langle 1| \alpha |0\rangle + \beta \langle 1 \,|\, 1\rangle \langle 1| \beta |1\rangle && (2.14)\\ &= \alpha^2 \langle 0 \,|\, 1\rangle \langle 1 \,|\, 0\rangle + \beta^2 \langle 1 \,|\, 1\rangle \langle 1 \,|\, 1\rangle && (2.15)\\ &= \beta^2 && (2.16) \end{aligned}$$

as $M_i^\dagger M_i = M_i$ and $\langle i \,|\, j\rangle = \delta_{ij}$.

After the measurement, the state of the qubit will be either

$$\begin{aligned} \left|\psi^\dagger\right\rangle &= \frac{M_0 |\psi\rangle}{\sqrt{p(0)}} && (2.17)\\ &= \frac{|0\rangle\langle 0| (\alpha |0\rangle + \beta |1\rangle)}{\sqrt{\alpha^2}} && (2.18)\\ &= \frac{\alpha |0\rangle \langle 0 \,|\, 0\rangle + \beta |0\rangle \langle 0 \,|\, 1\rangle}{\alpha} && (2.19)\\ &= \frac{\alpha |0\rangle}{\alpha} && (2.20)\\ &= |0\rangle && (2.21) \end{aligned}$$

or

$$\left|\psi^{\dagger}\right\rangle = \frac{M_1 \left|\psi\right\rangle}{\sqrt{p(1)}} \tag{2.22}$$

$$= \frac{\left|1\right\rangle \left\langle 1\right| \left(\alpha \left|0\right\rangle + \beta \left|1\right\rangle\right)}{\sqrt{\beta^2}} \tag{2.23}$$

$$= \frac{\alpha \left|1\right\rangle \left\langle 1 \,|\, 0\right\rangle + \beta \left|1\right\rangle \left\langle 1 \,|\, 1\right\rangle}{\beta} \tag{2.24}$$

$$= \frac{\beta \left|1\right\rangle}{\beta} \tag{2.25}$$

$$= \left|1\right\rangle \tag{2.26}$$

respectively, implying that the state of the qubit collapsed into one of the two computational basis states. Thus, any succinct measurement will result in the same outcome. In order to perform multiple measurements on the same state, it has to be prepared multiple times.

Two special qubit states, which often occur in the domain of quantum computation, are the $|-\rangle$ and $|+\rangle$ state defined as:

$$\left|-\right\rangle = \frac{1}{\sqrt{2}} \cdot \left|0\right\rangle - \frac{1}{\sqrt{2}} \cdot \left|1\right\rangle \tag{2.27}$$

and

$$\left|+\right\rangle = \frac{1}{\sqrt{2}} \cdot \left|0\right\rangle + \frac{1}{\sqrt{2}} \cdot \left|1\right\rangle . \tag{2.28}$$

Those states differ in a *relative phase*. Both have the same measurement statistics, lying between the states $|0\rangle$ and $|1\rangle$ on the Bloch Sphere:

$$p(0) = \left\langle +\right| M_0 \left|+\right\rangle \tag{2.29}$$

$$= \frac{1}{\sqrt{2}} \left\langle 0 \,|\, 0\right\rangle \left\langle 0\right| \frac{1}{\sqrt{2}} \left|0\right\rangle + \frac{1}{\sqrt{2}} \left\langle 1 \,|\, 0\right\rangle \left\langle 0\right| \frac{1}{\sqrt{2}} \left|1\right\rangle \tag{2.30}$$

$$= \frac{1}{2} \left\langle 0 \,|\, 0\right\rangle \left\langle 0 \,|\, 0\right\rangle + \frac{1}{2} \left\langle 1 \,|\, 0\right\rangle \left\langle 0 \,|\, 1\right\rangle \tag{2.31}$$

$$= \frac{1}{2} \tag{2.32}$$

and

$$p(1) = \langle +| M_1 |+\rangle \tag{2.33}$$
$$= \frac{1}{\sqrt{2}} \langle 0 \,|\, 1\rangle \langle 1| \frac{1}{\sqrt{2}} |0\rangle + \frac{1}{\sqrt{2}} \langle 1 \,|\, 1\rangle \langle 1| \frac{1}{\sqrt{2}} |1\rangle \tag{2.34}$$
$$= \frac{1}{2} \langle 0 \,|\, 1\rangle \langle 1 \,|\, 0\rangle + \frac{1}{2} \langle 1 \,|\, 1\rangle \langle 1 \,|\, 1\rangle \tag{2.35}$$
$$= \frac{1}{2} \tag{2.36}$$

for the $|+\rangle$ state. The same probabilities hold for the $|-\rangle$ state. Again, the state will be destroyed on measurement and be either $|0\rangle$ or $|1\rangle$ afterward, depending on the measurement outcome.

2.2 Multiple Qubits and Entanglement

The state vector of a single qubit lies in a two-dimensional space, assigning a complex-valued amplitude to each of the both possible measurement outcomes $|0\rangle$ and $|1\rangle$. The state vector of a multi-qubit system is defined by the *tensor product* of the state vectors of the individual subsystems. For a two-qubit system consisting of $|\psi_1\rangle = \alpha_1 |0\rangle + \beta_1 |1\rangle$ and $|\psi_2\rangle = \alpha_2 |0\rangle + \beta_2 |1\rangle$, the state vector is given by:

$$|\psi_{1,2}\rangle = |\psi_1\rangle \otimes |\psi_2\rangle \tag{2.37}$$
$$= (\alpha_1 |0\rangle + \beta_1 |1\rangle) \otimes (\alpha_2 |0\rangle + \beta_2 |1\rangle) \tag{2.38}$$
$$= \alpha_1\alpha_2 |0\rangle |0\rangle + \alpha_1\beta_2 |0\rangle |1\rangle + \beta_1\alpha_2 |1\rangle |1\rangle + \beta_1\beta_2 |1\rangle |1\rangle \tag{2.39}$$
$$= \alpha_1\alpha_2 |00\rangle + \alpha_1\beta_2 |01\rangle + \beta_1\alpha_2 |10\rangle + \beta_1\beta_2 |11\rangle \tag{2.40}$$
$$= \alpha_1\alpha_2 |0\rangle + \alpha_1\beta_2 |1\rangle + \beta_1\alpha_2 |2\rangle + \beta_1\beta_2 |3\rangle , \tag{2.41}$$

where $|0\rangle = |00\rangle$, $|1\rangle = |01\rangle$, $|2\rangle = |10\rangle$ and $|3\rangle = |11\rangle$. In general, the wave function of a n-qubit system is given by a 2^n dimensional vector:

$$|\psi\rangle = \sum_{i=0}^{2^n} a_i |i\rangle . \tag{2.42}$$

Therefore, a classical simulation of a n-dimensional qubit system has to keep track of 2^n complex amplitudes. This makes it impossible to simulate quantum systems above a certain size. For the classical simulation of a system consisting of 500 qubits, the state vector's dimension is already larger than the number of atoms in the universe.

As in the single qubit case, the probability to observe state $|n\rangle$ is given by a_n^2. It is also possible to only measure a subset of the qubits, leaving the other qubits in the normalized state:

$$|\psi\prime\rangle = \frac{(M_m \otimes I)\,|\psi\rangle}{\sqrt{p(m)}}. \tag{2.43}$$

A phenomenon that can appear in multi-qubit systems is *entanglement*. Consider for instance the two-qubit state

$$|\psi\rangle = \frac{|00\rangle + |11\rangle}{\sqrt{2}}. \tag{2.44}$$

This state can be created with a very simplistic quantum program as shown later in section **??**. Note that this state is a proper two-qubit state as it fulfills the normalization property $a_{00}^2 + a_{11}^2 = \frac{1}{\sqrt{2}}^2 + \frac{1}{\sqrt{2}}^2 = \frac{1}{2} + \frac{1}{2} = 1$.

Nevertheless, there are no two single-qubit states $|a\rangle$ and $|b\rangle$ such that $|\psi\rangle = |a\rangle\,|b\rangle$. The two qubits of $|\psi\rangle$ are *entangled* with each other. Measuring one of the qubits immediately determines the state of the other qubit, i.e. measuring the first qubit as $|0\rangle$ happens with probability:

$$\begin{aligned} p_1(0) &= \langle\psi|\,(M_0 \otimes I)^\dagger (M_o \otimes I)\,|\psi\rangle && (2.45)\\ &= \frac{1}{\sqrt{2}}\,\langle 00|\,\frac{1}{\sqrt{2}}\,|00\rangle && (2.46)\\ &= \frac{1}{2}, && (2.47) \end{aligned}$$

leaving the system in the post-measurement state:

$$\begin{aligned} |\psi\prime\rangle &= \frac{(M_0 \otimes I)\psi}{\sqrt{p_1(0)}} && (2.48)\\ &= \frac{\frac{1}{\sqrt{2}}\,|00\rangle}{\frac{1}{\sqrt{2}}} && (2.49)\\ &= |00\rangle\,. && (2.50) \end{aligned}$$

The same maths apply for the case of measuring the first qubit as $|1\rangle$.

Even if the state of the second qubit is not determined before, it will be either $|0\rangle$ or $|1\rangle$ from the moment on the *other* qubit has been measured.

The exponential growth of the state space dimension and entanglement are two properties of quantum systems which make them hard to simulate classically. Known quantum algorithms with quantum speedups like Shor's algorithm create entanglement in smart ways to perform calculations which seem to be impossible for classical computers.

2.3 Quantum Gates

It is physically possible to modify the state vector of a quantum system, even when it is in a coherent state. This opens the theoretical possibility to perform calculations based on the laws of quantum physics and build quantum computers.

The quantum state can be modified through *quantum gates*. Quantum physics allows the gates only to be linear and reversible. Thus, quantum gates can be mathematically described as unitary matrices. Gates vary in the number of qubits on which they act and the effects they have on the qubits' state.

2.3.1 Single-Qubit Gates

Single qubit gates are linear mappings that can be applied to the state vector of a single qubit. Mathematically, single-qubit gates can be described by 2×2 unitary matrices. The fact that these matrices are unitary makes sure the state $|\phi\rangle = G\,|\psi\rangle$ after gate G has been applied to state $|\psi\rangle$ is a proper quantum state which preserves the normalization constraint $\alpha^2_{|\phi\rangle} + \beta^2_{|\phi\rangle} = 1$.

An example of a single qubit gate is the NOT or X gate, also denoted as:

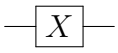

or

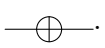

.

The X gate is the quantum analog of the classical NOT gate. Like the classical version, the X gate swaps the states $|0\rangle$ and $|1\rangle$ when applied to them. It is even more general, as it maps a single-qubit state of the form

$$|\psi\rangle = \alpha\,|0\rangle + \beta\,|1\rangle \tag{2.51}$$

to the state

$$|\phi\rangle = \beta\,|0\rangle + \alpha\,|1\rangle \tag{2.52}$$

by swapping the amplitudes for $|0\rangle$ and $|1\rangle$. The X gate has the following matrix representation:

$$X = \begin{pmatrix} 0 & 1 \\ 1 & 0 \end{pmatrix}. \tag{2.53}$$

A single qubit gate is applied to a quantum state by matrix multiplication:

$$|\phi\rangle = X|\psi\rangle \tag{2.54}$$
$$= \begin{pmatrix} 0 & 1 \\ 1 & 0 \end{pmatrix} |\psi\rangle \tag{2.55}$$
$$= \begin{pmatrix} 0 & 1 \\ 1 & 0 \end{pmatrix} \begin{pmatrix} \alpha \\ \beta \end{pmatrix} \tag{2.56}$$
$$= \begin{pmatrix} \beta \\ \alpha \end{pmatrix} \tag{2.57}$$

Another example of a single qubit gate without any classical analog is the *Hadamard gate* or H gate, described by the unitary:

$$H = \frac{1}{\sqrt{2}} \begin{pmatrix} 1 & 1 \\ 1 & -1 \end{pmatrix}. \tag{2.58}$$

Notice that the H gate is a unitary as it is reversible:

$$H^\dagger H = I. \tag{2.59}$$

The Hadamard gate maps between the so-called Z and X bases, mapping the states:

$$H|0\rangle = |+\rangle \tag{2.60}$$
$$H|1\rangle = |-\rangle \tag{2.61}$$

and back

$$H|+\rangle = |0\rangle \tag{2.62}$$
$$H|-\rangle = |1\rangle. \tag{2.63}$$

The Hadamard gate is a good example of how the Bloch Sphere visualization can help to understand a qubit state's transformation. The application of the Hadamard gate to the $|+\rangle$ is shown in figure **??**.

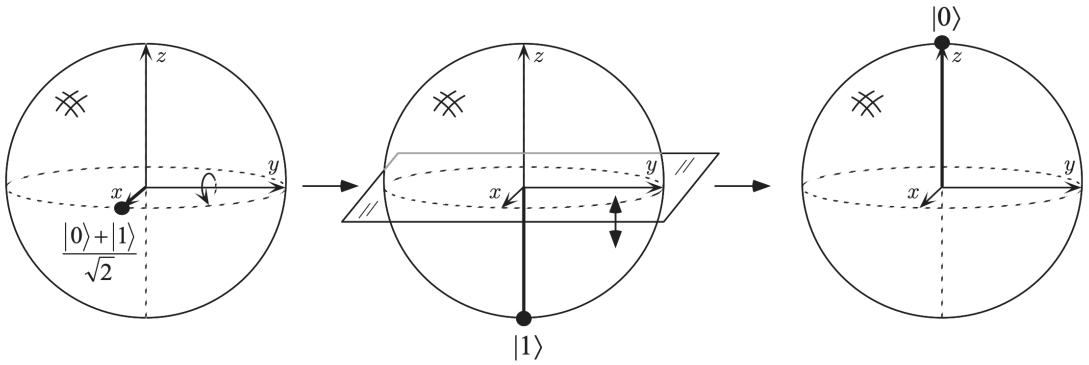

Figure 2.2: Visualization of the Hadamard gate on the Bloch sphere, acting on the $|+\rangle$ state [27].

An overview of some common single-qubit gates is given in figure **??**.

uu Operator	Gate	Matrix
X	X	$\begin{pmatrix} 0 & 1 \\ 1 & 0 \end{pmatrix}$
Y	Y	$\begin{pmatrix} 0 & -i \\ i & 0 \end{pmatrix}$
Z	Z	$\begin{pmatrix} 1 & 0 \\ 0 & -1 \end{pmatrix}$
H	H	$\frac{1}{\sqrt{2}}\begin{pmatrix} 1 & 1 \\ 1 & -1 \end{pmatrix}$
S	S	$\begin{pmatrix} 1 & 0 \\ 0 & i \end{pmatrix}$
T	T	$\begin{pmatrix} 1 & 0 \\ 0 & e^{i\frac{\pi}{2}} \end{pmatrix}$

Table 2.1: Overview of common single-qubit gates.

There are indefinitely many possible quantum gates in theory. Still, a universal finite gate set consisting of a few gates is sufficient to construct arbitrary unitary transformations [23]. This is the same as in the classical case where NAND gates suffice to build up arbitrary classical computation circuits [31] and good news for the fabrication of quantum computers with reusable components.

Nevertheless, single-qubit gates are not sufficient to build all possible unitary transformations on multi-qubit systems. For this purpose, multi-qubit gates are a necessity.

2.3.2 Multi-Qubit Gates

Single-qubit gates are not sufficient to create universal gate sets for quantum computation. In order to run arbitrary quantum programs, multi-qubit gates like *controlled* gates are needed. Controlled quantum gates are simple extensions of single-qubit gates. Every single-qubit gate can be implemented as a controlled version of it with one *control* and one *target* qubit. Only if the control qubit is in the $|1\rangle$ state, the gate is applied to the target qubit. As the control qubit can be in a superposition state, it is possible to apply and not apply the gate to the target qubit at the same time.

The prototypical two-qubit gate is the controlled NOT or CNOT gate. It is the controlled version of the X gate described before. As the CNOT gate acts on a two-qubit state, it can be described by a 4×4 unitary matrix. Each column describes the mapping of one of the four base state $|00\rangle$, $|01\rangle$, $|10\rangle$ and $|11\rangle$. The matrix representation of the CNOT gate is the following:

$$CNOT = \begin{pmatrix} 1 & 0 & 0 & 0 \\ 0 & 1 & 0 & 0 \\ 0 & 0 & 0 & 1 \\ 0 & 0 & 1 & 0 \end{pmatrix}. \tag{2.64}$$

The matrix can be read as follows: The first two columns describe that the vectors $|00\rangle$ and $|01\rangle$ will not change when the gate is applied to these states. Only when the first qubit is in the $|1\rangle$ state, will the state of the second qubit be swapped. Thus $|10\rangle$ will be mapped to $|11\rangle$ and $|11\rangle$ to $|10\rangle$.

This shows how the matrix representation of generalized two-qubit gates can be derived: As long as the control qubit is off, it does not affect the state. Thus, the controlled gate matrix is the same as the identity with 1s on the diagonal and 0s elsewhere in the upper left corner. Only when the first qubit is in the $|1\rangle$ state, the matrix differs from the identity. For example, the controlled version of the Z gate:

$$Z = \begin{pmatrix} 1 & 0 \\ 0 & -1 \end{pmatrix} \tag{2.65}$$

is given by:

$$CZ = \begin{pmatrix} 1 & 0 & 0 & 0 \\ 0 & 1 & 0 & 0 \\ 0 & 0 & 1 & 0 \\ 0 & 0 & 0 & -1 \end{pmatrix}. \tag{2.66}$$

A controlled gate G is represented by a vertical line ending in a black dot indicating the control qubit:

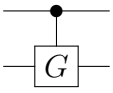

With two-qubit operations at hand, it is possible to build a universal gate set. A commonly used gate set is the so-called *Clifford + T* set, consisting of the gates $CNOT$, H, S and T [15]. The Solovay-Kitaev theorem [23] guarantees that this set can efficiently approximate any unitary operation. In this study, another universal gate set will be used, composed of the CZ, $\sqrt{X}$, $\sqrt{Y}$ and T gates [2].

2.4 Quantum Circuits

The standard model for computation in theoretical computer science is the Turing Machine [36]. Invented by Alan Turing in 1936, it is a powerful tool to understand the limits of (classical) computation. The theoretical nature of the Turing machine gives it unlimited computational resources, like infinite memory, which do not reflect the properties of realizable computer architectures.

Another computation model that does not suffer from the gap between theory and practice is the *circuit model* [30]. In the classical circuit model, each bit is represented by a wire, and operations (or gates) are represented by different shapes acting on those wires. The circuit model is as powerful as a Turing Machine. It is the model of choice in quantum computing.

Quantum programs are described by quantum circuits. Each qubit is represented by a wire and each gate by a rectangular on those wires. Figure **??** describes a very simple quantum circuit which flips a single qubit initialized in the $|0\rangle$ state by applying a X gate before measuring it.

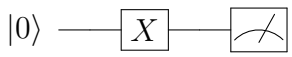

Figure 2.3: A simple quantum circuit applying an X gate to a qubit initialized in the $|0\rangle$ state before measuring it.

The circuit is being read from left to right. Important to note is that for calculating the resulting state, the matrix representation of the gates are multiplied from the left side to the current state $|\psi\rangle$ In the example above the final state of the program represented at the end of the circuit is:

$$|\phi\rangle = X\,|\psi\rangle \tag{2.67}$$
$$= \begin{pmatrix} 0 & 1 \\ 1 & 0 \end{pmatrix} |\psi\rangle \tag{2.68}$$
$$= \begin{pmatrix} 0 & 1 \\ 1 & 0 \end{pmatrix} \begin{pmatrix} \alpha \\ \beta \end{pmatrix} \tag{2.69}$$
$$= \begin{pmatrix} \beta \\ \alpha \end{pmatrix}. \tag{2.70}$$

In practice, circuits consist of several qubits and multiple gates, that are applied to them. It is possible to apply gates to different qubits sequentially as well as in parallel, as demonstrated in figure **??**:

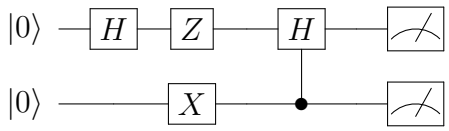

Figure 2.4: A quantum circuit acting on two qubits. The effect of parallel applications of single-qubit gates is defined by the tensor product of the gates.

Note that, when calculating the state of the quantum program above, the state of the system is given by the tensor product of the individual qubit states. For the circuit from figure **??**, the initial state $|\psi_{init}\rangle$ before any gate has been applied is:

$$|\psi_{init}\rangle = |0\rangle \otimes |0\rangle \tag{2.71}$$
$$= \begin{pmatrix} 1 \\ 0 \end{pmatrix} \otimes \begin{pmatrix} 1 \\ 0 \end{pmatrix} \tag{2.72}$$
$$= \begin{pmatrix} 1 \\ 0 \\ 0 \\ 0 \end{pmatrix} \tag{2.73}$$
$$= |00\rangle\,. \tag{2.74}$$

When a gate gets applied to only a subset of the qubits, as in the case of the first H gate in the circuit above, the unitary applied to the multi-qubit state is implicitly the tensor product of the gate on that qubit and identity matrices on the remaining qubits. For the given circuit, the state $|\psi_{H_1}\rangle$ after the first H gate on the first qubit is calculated as:

$$|\psi_{H_1}\rangle = (H \otimes I)\,|00\rangle \tag{2.75}$$

$$= \left(\frac{1}{\sqrt{2}}\begin{pmatrix}1 & 1\\ 1 & -1\end{pmatrix} \otimes \begin{pmatrix}1 & 0\\ 0 & 1\end{pmatrix}\right)|00\rangle \tag{2.76}$$

$$= \frac{1}{\sqrt{2}}\begin{pmatrix}1 & 0 & 1 & 0\\ 0 & 1 & 0 & 1\\ 1 & 0 & -1 & 0\\ 0 & 1 & 0 & -1\end{pmatrix}|00\rangle \tag{2.77}$$

$$= \frac{1}{\sqrt{2}}\begin{pmatrix}1 & 0 & 1 & 0\\ 0 & 1 & 0 & 1\\ 1 & 0 & -1 & 0\\ 0 & 1 & 0 & -1\end{pmatrix}\begin{pmatrix}1\\ 0\\ 0\\ 0\end{pmatrix} \tag{2.78}$$

$$= \frac{1}{\sqrt{2}}\begin{pmatrix}1\\ 0\\ 1\\ 0\end{pmatrix} \tag{2.79}$$

$$= |+0\rangle\,. \tag{2.80}$$

As expected, applying a H gate to the first qubit, it should be in the $|+\rangle$ state while the second qubit remains in the $|0\rangle$ state.

Similar to the first gate, the unitary applied to the state, when multiple gates are applied to different qubits at the same time, is constructed by the tensor product of those gates. The resulting state $|\psi_{Z_1X_2}\rangle$ after the Z gate is applied to the first qubit, and the X gate is applied to the second qubit, is calculated as:

$$
\begin{aligned}
|\psi_{Z_1X_2}\rangle &= (Z \otimes X)\,|+0\rangle && (2.81)\\
&= \left(\begin{pmatrix}1 & 0\\ 0 & -1\end{pmatrix} \otimes \begin{pmatrix}0 & 1\\ 1 & 0\end{pmatrix}\right)|+0\rangle && (2.82)\\
&= \begin{pmatrix}0 & 1 & 0 & 0\\ 1 & 0 & 0 & 0\\ 0 & 0 & 0 & -1\\ 0 & 0 & -1 & 0\end{pmatrix}|+0\rangle && (2.83)\\
&= \begin{pmatrix}0 & 1 & 0 & 0\\ 1 & 0 & 0 & 0\\ 0 & 0 & 0 & -1\\ 0 & 0 & -1 & 0\end{pmatrix}\begin{pmatrix}\frac{1}{\sqrt{2}}\\ 0\\ \frac{1}{\sqrt{2}}\\ 0\end{pmatrix} && (2.84)\\
&= \begin{pmatrix}0\\ \frac{1}{\sqrt{2}}\\ 0\\ -\frac{1}{\sqrt{2}}\end{pmatrix} && (2.85)\\
&= |-1\rangle\,. && (2.86)
\end{aligned}
$$

Accordingly, applying a Z gate to the $|+\rangle$ state brings the first qubit to the $|-\rangle$ state, while the X gate on the second qubit moves the qubit state from the $|0\rangle$ to the $|1\rangle$ state.

The final state $|\psi_{final}\rangle$ of the circuit is calculated by applying the 4×4 matrix representation of the controlled H gate to $|-1\rangle$. In this case, the second qubit is the controlled qubit:

$$|\psi_{final}\rangle = CH\,|-1\rangle \tag{2.87}$$

$$= \begin{pmatrix} 1 & 0 & 0 & 0 \\ 0 & \frac{1}{\sqrt{2}} & 0 & \frac{1}{\sqrt{2}} \\ 0 & 0 & 1 & 0 \\ 0 & \frac{1}{\sqrt{2}} & 0 & -\frac{1}{\sqrt{2}} \end{pmatrix} |-1\rangle \tag{2.88}$$

$$= \begin{pmatrix} 1 & 0 & 0 & 0 \\ 0 & \frac{1}{\sqrt{2}} & 0 & \frac{1}{\sqrt{2}} \\ 0 & 0 & 1 & 0 \\ 0 & \frac{1}{\sqrt{2}} & 0 & -\frac{1}{\sqrt{2}} \end{pmatrix} \begin{pmatrix} 0 \\ \frac{1}{\sqrt{2}} \\ 0 \\ -\frac{1}{\sqrt{2}} \end{pmatrix} \tag{2.89}$$

$$= \begin{pmatrix} 0 \\ 0 \\ 0 \\ 1 \end{pmatrix} \tag{2.90}$$

$$= |11\rangle\,. \tag{2.91}$$

The first qubit has been swapped from the $|-\rangle$ to the $|1\rangle$ state as the second qubit is in the $|1\rangle$ state and the H gate has been applied. The circuit **??** thus maps the initial state $|00\rangle$ to $|11\rangle$.

Another simple quantum circuit, which entangles two qubits with each other, is shown in figure **??**.

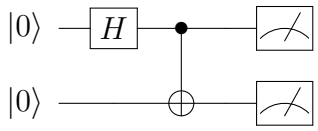

Figure 2.5: A quantum circuit to create maximally entangled 2-qubit states.

The Hadamard gate on the first qubit maps the system from the initial $|00\rangle$ into the $|+0\rangle$ state. Afterward, the first qubit, which is currently between the $|0\rangle$ and $|1\rangle$ state on the Bloch Sphere, is used as the control qubit in the $CNOT$ gate. This has an interesting effect on the second qubit, as the X gate is applied and not applied at the same time, entangling the two qubits with each other. The final state before measurement is $\frac{|00\rangle+|11\rangle}{2}$, which has been discussed in section **??**. This state is also known as one of the four *Bell states*. They represent maximally entangled two-qubit states. Moreover, they play an important role in the analysis of *quantum communication*.

The quantum circuit demonstrates how entanglement can be created by applying controlled gates with qubits in superposition states. Entanglement plays an essential role in the construction of so-called *random quantum circuits* in recent quantum supremacy experiments.

2.5 Quantum Computational Complexity

It is essential to understand the theoretical capabilities and limitations of quantum computers to understand for which kind of problems they provide advantages over classical computers.

For many years, it has been assumed that the extended Church Turing thesis holds true. It states that a probabilistic Turing machine can efficiently simulate any realistic model of computation. The thesis is challenged by quantum computers, because they can potentially solve specific problems exponentially faster than classical computers [11].

The class of problems which can be solved efficiently by a quantum computer is called **BQP**, shorthand for *bounded-error quantum polynomial time* [5]. A decision problem is in **BQP** if there exists a quantum program that solves the decision problem in 2/3 of the cases and runs in polynomial time. This is the quantum analog of the *bounded-error probabilistic polynomial time* or **BPP** [14], which is decidable by a probabilistic Turing machine in polynomial time and widely believed to be the same as **P**.

Currently, there are a few problems known to be in **BQP**, which are suspected not to be in **P**, providing evidence for the superiority of quantum computers. One of these problems is *factorization*, the problem of decomposing a composite integer into its prime factors. This problem has been known to be in *NP* before. Though, it is also known that factorization is not an **NP**-hard problem, indicating that quantum computers are not able to provide an exponential speedup for every problem that is not efficiently solvable on a classical computer. Indeed, classical algorithms might even exist, which can solve factorization on a classical computer efficiently, which have not been discovered yet.

While **BQP** includes **P** and intersects with **NP**, it can be shown that it is strictly included in **PSPACE** [5]. The relationship of these complexity classes is visualized in figure 2.6.

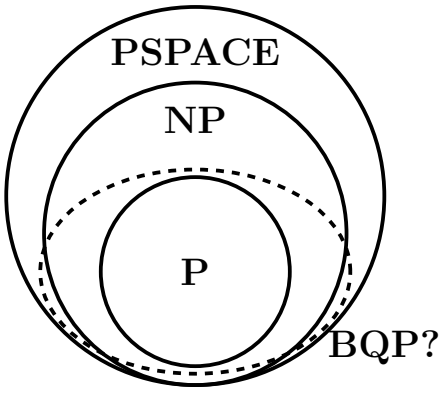

Figure 2.6: Relation of Complexity Classes to each other.

While it is hard to prove some fundamental relationships between complexity

classes like the famous $\mathbf{P} \stackrel{?}{=} \mathbf{NP}$ problem, it is believed that quantum computers can solve specific problems with practical applications like integer factorization [32] or the simulation of quantum systems [11] exponentially faster than classical computers.

The moment in time a physical quantum computer can outperform a classical computer on a specific problem for the first time has been coined by John Preskill in 2012 as *quantum supremacy* [28]. Recently, Google announced their quantum supremacy results with a 54 qubit quantum computer, providing the first physical evidence that it might be possible to build quantum computers with advantages over classical computers [2].

3 Boltzmann Machines

The following chapter gives an introduction to Boltzmann machines and their applications to the classical simulation of quantum computing.

An overview of the architecture and mathematical properties of Boltzmann machines are given in the first section. The restricted Boltzmann machine is motivated as a special kind of Boltzmann machine with useful mathematical properties in the second part of this chapter. Afterward, the concepts of Gibbs sampling and supervised learning are explained. In the last section, a constructive approach is given on how restricted Boltzmann machines can be applied to the classical simulation of quantum computing.

The introduction to Boltzmann machines and restricted Boltzmann machines as well as the introduction to Gibbs sampling are based on [25] and [12] which provide a more throughout introduction into the topic. The work of Jónsson, Bauer and Carleo [21] is the foundation of the last section of this chapter.

3.1 Characteristics

The concept of the Boltzmann machine has first been proposed in the 1980s as a model for parallel distributed computing [20]. Boltzmann machines are physically inspired by the Ising Spin model and can be interpreted as energy-based recurrent neural networks representing probability distributions over vectors $\boldsymbol{d}_i \in \{0,1\}^n$ [1].

A Boltzmann machine is a network of stochastic units (or neurons) $X = V \cup H$ which are segmented into *visible* neurons $V = \{v_1, \ldots, v_n\}$ and *hidden* neurons $H = \{h_1, \ldots, h_m\}$. The joint state of the visible neurons $\boldsymbol{v} = (v_1 \ldots v_n) \in \{0,1\}^n$ represents n-dimensional data points $\boldsymbol{d}_i \in \{0,1\}^n$. The hidden neurons increase the expressiveness of the Boltzmann machine by acting as non-linear feature detectors to model dependencies between the visible neurons [17].

The neurons are connected to each other by weighted links W_{ij} and poss biases a_i (visible) or b_i (hidden), respectively. In general, the neurons of such a Boltzmann machine can be fully connected. A graphical representation of a fully connected Boltzmann machine is shown in figure **??**.

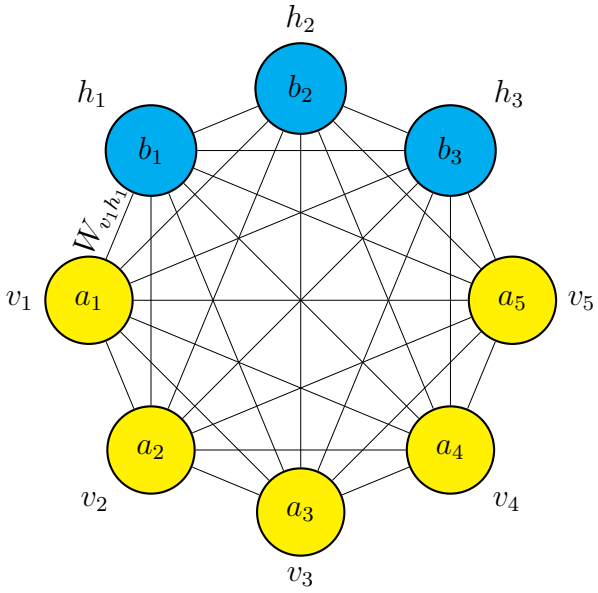

Figure 3.1: Graphical representation of a fully connected Boltzmann machine with 5 visible neurons (yellow) v_1 to v_5 and 3 hidden neurons (blue) h_1 to h_3. Each neuron posses a bias a_1 to a_5 and b_1 to b_3 respectively. The connection weight between two neurons i and j is given by W_{ij}.

Each configuration $\boldsymbol{c} = (v_1, \ldots, v_n, h_1, \ldots, h_m)$ of neuron states of the Boltzmann machine is associated with an energy $E(\boldsymbol{c})$ value, which is defined by the parameters $\mathcal{W}$, consisting of the weights and biases $\mathcal{W} = \{a_i, b_i, W_{ij}\}$:

$$E(\boldsymbol{c}; \mathcal{W}) = -\sum_{v_i \in V} a_i v_i - \sum_{h_i \in H} b_i h_i - \sum_{x_i, x_j \in X} W_{x_i, x_j} x_i x_j. \tag{3.1}$$

When sampling configurations from the Boltzmann machine (discussed in more detail in section 3.3), the Boltzmann machine prefers low energy states over states with high energies. The *stationary probability* of a configuration $\boldsymbol{c}$ with energy $E(\boldsymbol{c}; \mathcal{W})$ is given by the so-called *Gibbs-Boltzmann distribution* [13]:

$$p(\boldsymbol{c}; \mathcal{W}) = \frac{\mathrm{e}^{-E(\boldsymbol{c}; \mathcal{W})}}{Z(\mathcal{W})}, \tag{3.2}$$

where $Z(\mathcal{W})$ is the normalizing partition function

$$Z(\mathcal{W}) = \sum_{\boldsymbol{c\prime} \in C} \mathrm{e}^{-E(\boldsymbol{c\prime}; \mathcal{W})}. \tag{3.3}$$

In a training phase (discussed in section 3.4), the parameters of the Boltzmann machine can be adapted in such a way that the marginal probability distribution $p(\boldsymbol{v}; \mathcal{W})$ of the visible neurons

$$p(\boldsymbol{v}; \mathcal{W}) = \sum_{\boldsymbol{h}_k \in \{0,1\}^m} p(\boldsymbol{v}, \boldsymbol{h}_k; \mathcal{W}), \tag{3.4}$$

which traces out the hidden unit states by summing over all possible configurations of them, resembles the probability distribution of data points $\boldsymbol{d}_i$ in a training set $D = \{\boldsymbol{d}_1, \ldots, \boldsymbol{d}_l\}$.

For a fully connected Boltzmann machine, this representation consists of an exponential number of summands and cannot be calculated efficiently. So-called *Restricted Boltzmann Machines* have a specific architecture with a restricted connectivity, which allows the efficient calculation of the marginal probability.

3.2 Restricted Boltzmann Machines

The Restricted Boltzmann machine (RBM) is a type of Boltzmann machine with a specific architecture and properties [33]. Since their invention, RBMs have been applied to a variety of machine learning tasks. They played a key role in the development of deep learning architectures as building blocks of so-called Deep Belief networks [4, 19]. RBMs are also the kind of Boltzmann machines which are being used in this study of the simulation of quantum circuits.

In its restricted form, the neurons of the Boltzmann machine are separated into two layers; one being the visible layer containing the visible neurons $v_i \in V$ and the other layer being the hidden layer containing the hidden neurons $h_j \in H$. Each neuron of the RBM is only allowed to be connected to the neurons from the other layer. Intra-layer connections are not allowed. As a result, the graph of the RBM is bipartite, as shown in figure **??**.

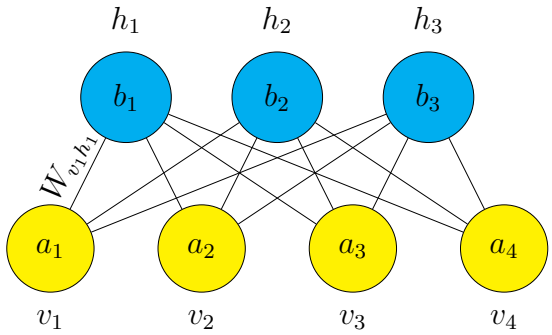

Figure 3.2: Graphical representation of a RBM with 5 visible neurons and 3 hidden ones. There are only connections between the two layers and no connection between two neurons from the same layer.

The marginal probability $p(\boldsymbol{v}; \mathcal{W})$ of the visible neuron states in a RBM has the form:

$$p(\boldsymbol{v};\mathcal{W}) = \sum_{\boldsymbol{h}_k\in\{0,1\}^m} p(\boldsymbol{v},\boldsymbol{h}_k;\mathcal{W}) \tag{3.5}$$

$$= \frac{1}{Z(\mathcal{W})} \sum_{\boldsymbol{h}_k\in\{0,1\}^m} \mathrm{e}^{-E(\boldsymbol{v},\boldsymbol{h}_k;\mathcal{W})} \tag{3.6}$$

$$= \frac{1}{Z(\mathcal{W})} \sum_{h_1\in\{0,1\}} \cdots \sum_{h_m\in\{0,1\}} \mathrm{e}^{\sum_{v_i} b_i v_i} \prod_{j=1}^{m} \mathrm{e}^{h_j(b_j+\sum_{i=1}^{n} W_{ij}v_i)} \tag{3.7}$$

$$= \frac{\mathrm{e}^{\sum_{v_i} b_i v_i}}{Z(\mathcal{W})} \sum_{h_1\in\{0,1\}} \mathrm{e}^{h_1(b_1+\sum_{i=1}^{n} W_{i1}v_i)} \cdots \sum_{h_m\in\{0,1\}} \mathrm{e}^{h_m(b_m+\sum_{i=1}^{n} W_{im}v_i)} \tag{3.8}$$

$$= \frac{\mathrm{e}^{\sum_{v_i} b_i v_i}}{Z(\mathcal{W})} \prod_{i=1}^{m} \sum_{h_i\in\{0,1\}} \mathrm{e}^{h_i(b_i+\sum_{i=1}^{n} W_{ij}v_i)} \tag{3.9}$$

$$= \frac{\mathrm{e}^{\sum_{v_i} b_i v_i}}{Z(\mathcal{W})} \prod_{i=1}^{m} (1 + \mathrm{e}^{b_i+\sum_{i=1}^{n} W_{ij}v_i}). \tag{3.10}$$

This quantity consists of only a polynomial number of terms in the number of hidden units of the RBM. Consequently, it can be calculated efficiently. This makes the RBM a compact representation of a probability distribution over vectors $\boldsymbol{d}_i \in D$ inferred from a dataset D.

Even though the RBM has a limited connectivity between its units, it is a universal function approximator [24]. It can model any distribution over $\{0,1\}^m$ arbitrary well with m visible and k+1 hidden units, where k denotes the cardinality of the support set of the target distribution. That is the number of input elements from $\{0,1\}^m$ that have a non-zero probability of being observed. This also implies a worst-case exponential number of hidden units for distributions with an extensive support set [24]. Even fewer units can be sufficient depending on the patterns in the support set [26].

3.3 Gibbs Sampling

Boltzmann machines are generative models that represent probability distributions over their configurations. This means that it is possible to draw configurations from a Boltzmann machine according to their (marginal) probabilities given in equations 3.4 and 3.10.

Although it is required to calculate $Z(\mathcal{W})$ for the exact probabilities of each configuration, it is not necessary to calculate the energies for all 2^{n+m} possible configurations of a Boltzmann machine to draw samples from it.

Instead, Boltzmann machines can be seen as *Markov chains* with a stationary probability distribution. With a stochastic process called *Gibbs sampling*, the samples can be drawn efficiently according to this stationary distribution for

RBMs.

Gibbs sampling belongs to the class of so-called *Metropolis-Hastings* algorithms. By that, it is a *Monte Carlo Markov Chain* (MCMC) algorithm [16]. It is a simple algorithm to produce samples from the joint probability distribution of multiple random variables like neuron state configurations of a Boltzmann machine, which can be considered as a Markov chain.

A Markov chain is a discrete stochastic process of configurations of random variables $C = \{\boldsymbol{c}^{(t)}\}$ at time steps $t = 1, \ldots, T$ which take values in a set Ω (for Boltzmann machines $\Omega = \{0,1\}^{m+n}$) and for which for all time steps t and for all configurations $\boldsymbol{c}_j, \boldsymbol{c}_i, \boldsymbol{c}_{i-1}, \ldots, \boldsymbol{c}_0 \in \Omega$ the *Markov property*

$$p_{ij}^{(t)} := P(\boldsymbol{c}^{(t+1)} = c_j \mid \boldsymbol{c}^{(t)} = \boldsymbol{c}_i, \ldots, \boldsymbol{c}^{(0)} = c_0) \tag{3.11}$$

$$= P(\boldsymbol{c}^{(t+1)} = c_j \mid \boldsymbol{c}^{(t)} = \boldsymbol{c}_i) \tag{3.12}$$

holds. This means that the next state of the system only depends on the current state and not on the system's history. A Markov chain can be represented as a (finite) graph, as shown in figure **??**.

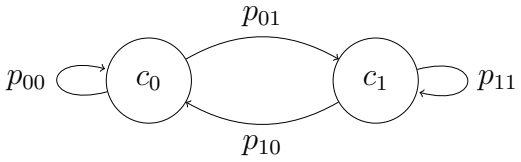

Figure 3.3: A Markov chain with two states c_0 and c_1. The Markov chain is described by the 2×2 matrix $\boldsymbol{P} = \begin{pmatrix} p_{00} & p_{01} \\ p_{10} & p_{11} \end{pmatrix}$.

In the case of Boltzmann machines, the transition probabilities p_{ij} are time independent and given by the ratios of configuration probabilities. For RBMs the transition probability p_{ij} from configuration c_i to c_j is given by:

$$p_{ij} = \frac{\mathrm{e}^{\sum_{v_i \in \boldsymbol{c_i}} b_i v_i} \prod_{i=1}^{m} (1 + \mathrm{e}^{b_i + \sum_{i=1}^{n} W_{ij} v_i})}{\mathrm{e}^{\sum_{v_i \in \boldsymbol{c_j}} b_i v_i} \prod_{i=1}^{m} (1 + \mathrm{e}^{b_i + \sum_{i=1}^{n} W_{ij} v_i})}, \tag{3.13}$$

which can be calculated efficiently as the $Z(\mathcal{W})$ terms from equation 3.10 cancel out.

In each time step t during the Gibbs sampling, the state of a single randomly chosen neuron of the RBM is flipped so that the configurations $\boldsymbol{c}^{(t)}$ and $\boldsymbol{c}^{(t+1)}$ only differ in the state of one neuron. With probability p_{ij} configuration $\boldsymbol{c}_j$ is kept as the new configuration. With probability $1 - p_{ij}$ the Boltzmann machine will stay in its current configuration $\boldsymbol{c}_i$. This corresponds to a random walk on the Markov chain defined by the RBM transition probabilities. The algorithm is given in algorithm **??**.

Algorithm 1 Gibbs Sampling

Require: $bm(c)$: function returning the energy of a Boltzmann machine for configuration c
Require: T: time steps
1: $t \leftarrow 0$
2: $c^{(0)} \leftarrow randomize(\{0,1\}^{m+n})$ (random initialization)
3: **repeat**
4: $\quad r \leftarrow random(m+n)$
5: $\quad E_i \leftarrow bm(c^{(t)})$
6: $\quad E_j \leftarrow bm(\{c_1, \ldots, \bar{c_r}, \ldots, c_{m+n}\})$
7: $\quad$ **if** $random(1) < \frac{E_i}{E_j}$ **then**
8: $\quad\quad c^{(t+1)} \leftarrow \{c_1, \ldots, \bar{c_r}, \ldots, c_{m+n}\}$
9: $\quad t \leftarrow t+1$
10: **until** $t = T$
11: **return** $c^{(T)}$

The Markov chain for configurations of a Boltzmann machine is known to converge to its so-called *stationary distribution* π, that is

$$\pi^T = \pi^T \boldsymbol{P} \tag{3.14}$$

with $\boldsymbol{P} = (p_{ij})$ being the transition matrix of the Markov chain with the transition probabilities as its entries. Once the Markov chain reaches its stationary distribution, all subsequent states will be distributed according to this distribution. Running Gibbs sampling for sufficiently many time steps T will sample configurations according to the Gibbs-Boltzmann distribution given in equation 3.10.

Although Gibbs sampling is a simple algorithm, it is an important algorithm in the context of Boltzmann machines. Different versions of Gibbs sampling have been developed for RBMs, like (persistent) contrastive divergence [18, 35] or parallel tempering [9]. In this study, Gibbs sampling will be used in its simplest version, as described in this chapter.

3.4 Supervised Learning

The probability distribution over vector spaces given by a Boltzmann machine can be trained to resemble the distribution of data points $\boldsymbol{d}_i$ in a dataset $D = \{\boldsymbol{d}_1, \ldots, \boldsymbol{d}_d\}$. This can be done either in a *unsupervised* or in a *supervised* manner.

In both cases the parameters $\mathcal{W} = \{\boldsymbol{a}, \boldsymbol{b}, \boldsymbol{W}\}$ of the Boltzmann machine are updated minimizing an objective function $O(\mathcal{W})$, which depends on the parameters of the Boltzmann machine and depicts the overlap of the current and the target distribution in an iterative process called *gradient descent*.

Before the training phase, the Boltzmann machine is initialized with random parameters $\theta_i \in \mathcal{W}_0$ and a training set $D = \{\boldsymbol{d}_1, \ldots, \boldsymbol{d}_d\}$ is given. In the case of

supervised learning of Boltzmann machines, the training set consists of tuples of configurations and their corresponding target energy values $\boldsymbol{d}_i = (\boldsymbol{c}_i, t_i)$.

In the batch version of gradient descent, the training set D is split into subsets $D_1, \ldots, D_l$, called *batches*.

For each such batch D_i, the average negative log overlap $\langle L(\mathcal{W}) \rangle$ for all $\boldsymbol{c}_j \in D_i$ is computed. Afterwards, the gradients $\frac{\partial L}{\partial \delta_i}$ are calculated and the parameters updated into the direction of the steepest descent:

$$\theta_i = \theta_i - \alpha \frac{\partial L}{\partial \delta_i} \tag{3.15}$$

with *learning rate* $\alpha \ll 1$ to keep the step sizes moderate. The learning rate prevents to big step sizes in steep areas of the objective function $L(\mathcal{W})$ This process is repeated for a defined number of iterations to minimize the objective function $O(\mathcal{W})$. A graphical representation of this process is shown in figure **??**.

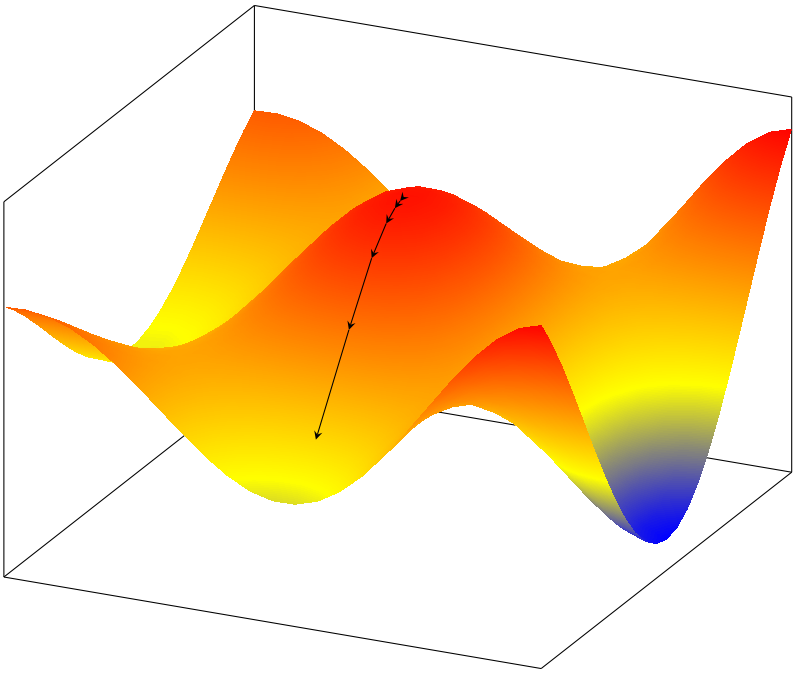

Figure 3.4: Iterations of a gradient descent method. At each iteration, the randomly initialized parameters get updated in direction of the steepest descent of the function to be optimized. After enough iterations, a minimum is of the function is reached.

The simple update rule in 3.15 has several drawbacks, however. First, The gradient and thus the step size will become smaller as closer the function approaches its minimum, leading to only small improvements and many steps necessary. Second, the function's shape will usually have (many) local minima, which should be avoided. Several variants of gradient descent have been developed to over-

come these issues [29]. Two of these methods are *AdaMax* [29] and *Stochastic Reconfiguration* [34].

3.4.1 Adamax

AdaMax is a special version of *Adam* [22].It combines the advantages of AdaGrad [10] and RMSProp [3], two other popular gradient descent methods. AdaMax is computationally efficient, has little memory requirements, and proves to be well suited for problems with much noise and sparse gradients.

Instead of using the raw gradient, the algorithm updates exponential moving averages of the gradient (mt) and the squared gradient (vt) to include more information about the shape of the error function into the parameter updates. The hyper-parameters $\beta_1, \beta_2 \in [0, 1)$ control the exponential decay rates of these moving averages. The moving averages themselves are estimates of the 1st moment (the mean) and the 2nd raw moment of the gradient. The update rule for the parameters θ_{ij} for Adamax are summarized in algorithm **??**.

Algorithm 2 Adamax

Require: α: step size
Require: $\beta_1, \beta_2 \in [0, 1)$: Exponential decay rates
Require: $f(\theta)$: Stochastic objective function with parameters $\theta_i \in \mathcal{W}$
Require: $\mathcal{W}_0$: Initial parameter vector
$m_0 \leftarrow 0$ (Initialize 1^{st} moment vector)
$u_0 \leftarrow 0$ (Initialize the exponential weighted infinity norm)
$t \leftarrow 0$ (Initialize time step)
while θ_t not converged **do**
    $t \leftarrow t + 1$
    $g_t \leftarrow \nabla_{\mathcal{W}} f_t(\mathcal{W}_{t-1})$ (Get gradients w.r.t. objective function at time step t)
    $m_t \leftarrow \beta_1 \cdot m_{t-1} + (1 - \beta_1) \cdot g_t$ (Update biased first moment estimate)
    $u_t \leftarrow max(\beta_2 \cdot u_{t-1}, |g_t)$ (Update the exponentially weighted infinity norm)
    $\mathcal{W}_t \leftarrow \mathcal{W}_{t-1} - (\alpha/(1 - \beta_1^t)) \cdot m_t/u_t$ (Update parameters)
return θ_t (Resulting parameters)

3.4.2 Stochastic Reconfiguration

Another popular gradient descent method to optimize the parameters of an RBM to represent quantum states is *Stochastic reconfiguration* []. The idea behind this method is that even a small change in the parameters of the RBM might lead to a big change in the output distribution of the RBM. Instead of small steps in the parameter space as in the pure version of gradient descent, the step size is kept small with respect to the change in the output distribution represented by the RBM. Stochastic reconfiguration is equivalent to the *natural gradient descent* method [].

The update rule for the parameters W of the RBM in the Stochastic Reconfiguration (SR) method is:

$$\theta_i' = \theta_i - \alpha \boldsymbol{S}^{-1} \boldsymbol{f} \tag{3.16}$$

with

$$\boldsymbol{f}_i = \langle \Delta_i^* \frac{\partial O}{\partial \theta_i} \rangle - \langle \Delta_i^* \rangle \langle \frac{\partial O}{\partial \theta_i} \rangle \tag{3.17}$$

$$\boldsymbol{S}_{ij} = \langle \Delta_i^* \Delta_j \rangle - \langle \Delta_i^* \rangle \langle \Delta_j \rangle \tag{3.18}$$

where $\langle x \rangle$ denotes the mean of a random variable x and Δ_i denotes the log-derivative of of the wave function $\Delta_i(\boldsymbol{c}) = \frac{1}{\psi(\boldsymbol{v})} \frac{\partial \psi(\boldsymbol{c})}{\partial \theta_i}$ with respect to some paramter $\theta_i \in \mathcal{W}$.

Using the covariance matrix $\boldsymbol{S}$ of the derivatives of the wave function keeps the KL divergence between the RBM before and after the update low, leading to a smooth transition through the error landscape [34].

Both AdaMax and Stochastic reconfiguration are modifications to the standard gradient descent method which try to reduce oscillations during the training and time to convergence by including more information about the shape of the error function into the changes of the gradients. This study will compare both methods for the classical simulation of quantum computing with RBMs.

3.5 Application to Quantum Computing

Machine learning techniques have become a successful approach for the classical simulation of quantum systems [7, 8, 6]. Carleo and Troyer [7] were the first to give a compact presentation of the wavefunction of a many-body quantum system with an RBM. The same framework has later been used by Jónsson, Bauer, and Carleo for the classical simulation of the quantum Fourier and Hadamard transform [21]. Their work gives a constructive approach on how the parameters of a complex-valued RBM representing the quantum state

$$|\psi_{\mathcal{W}}(\boldsymbol{v})\rangle = \frac{\mathrm{e}^{\sum_{v_i} b_i v_i}}{Z(\mathcal{W})} \prod_{i=1}^{m} (1 + \mathrm{e}^{b_i + \sum_{i=1}^{n} W_{ij} v_i}) \tag{3.19}$$

can be adapted to apply a universal set of quantum gates to the quantum state $|\psi_{\mathcal{W}}\rangle$.

RBMs allow an exact application only of unitary gates diagonal in the computational basis. For non-diagonal gates more hidden layers would be necessary, making the calculation of the quantum state intractable [6]. Nevertheless, it is possible to train a Boltzmann machine in a supervised fashion, such that its parameters are adapted to apply a non-diagonal gate to its state approximately.

The rules for the applications of diagonal and non-diagonal gates to an RBM state from [21] laid out in following two sections.

3.5.1 Diagonal Gates

Diagonal gates can be applied to an RBM quantum state by solving a set of linear equations. This section describes the rules for the applications of single-qubit Z rotations, controlled Z rotations as well as the Pauli X, Y and Z gates.

Single-Qubit Z rotations

The action of the single Z rotation of angle θ is given by the 2×2 unitary matrix

$$R_l^Z = \begin{pmatrix} 1 & 0 \\ 0 & \mathrm{e}^{i\theta} \end{pmatrix}. \tag{3.20}$$

Its action on qubit l yields $\langle \boldsymbol{v} \mid R_l^Z(\theta) \mid \psi_W \rangle = \mathrm{e}^{i\theta v_l} \left| \psi_W(\boldsymbol{v}) \right\rangle$. Considering a RBM machine with weights $\mathcal{W}' = \{\alpha', \beta', W'\}$, the action of the $R^Z(\theta)$ gate is exactly reproduced if $\mathrm{e}^{v_l a_l} \mathrm{e}^{i\theta v_l} = \mathrm{e}^{v_l a'_l}$ is satisfied. This is the case for

$$a'_j = a_j + \delta_{jl} i\theta. \tag{3.21}$$

The action of the Z rotation thus simply modifies the bias of the visible neuron l of the RBM.

Controlled Z rotations

The action of a controlled Z rotations acting on two given qubits l and m is determined by the 4×4 unitary matrix:

$$CZ = \begin{pmatrix} 1 & 0 & 0 & 0 \\ 0 & 1 & 0 & 0 \\ 0 & 0 & 1 & 0 \\ 0 & 0 & 0 & \mathrm{e}^{i\theta} \end{pmatrix} \tag{3.22}$$

where θ is a given rotation angle. This gate is diagonal and can compactly be written as

$$\langle \boldsymbol{v} \mid CZ(\theta) \mid \psi_W \rangle = \mathrm{e}^{i\theta v_l v_m} \left| \psi_W(v_1 \dots v_n) \right\rangle. \tag{3.23}$$

As the RBM architecture does not allow direct interaction between visible neurons, the CZ gate requires the insertion of a dedicated extra hidden unit h_c, which is connected to the qubits l and m:

$$\langle \boldsymbol{v} \mid CZ(\theta) \mid \psi_W \rangle = \mathrm{e}^{\Delta a_l B_l + \Delta a_m Z_m} \sum_{h_c} \mathrm{e}^{W_{lc} B_l h_c + W_{mc} B_m h_c} \tag{3.24}$$

$$= \mathrm{e}^{\Delta a_l B_l + \Delta a_m B_m} \times (1 + \mathrm{e}^{W_{lc} B_l + W_{mc}} B_m) \, |\psi_W(\boldsymbol{v})\rangle \,, \tag{3.25}$$

where the new weights W_{lc} and W_{mc} and visible units biases $a_l\prime = a_l + \Delta a_l$, $a_m\prime = a_m + \Delta a_m$ are determined by the equation:

$$\mathrm{e}^{\Delta a_l B_l + \Delta a_m B_m} (1 + \mathrm{e}^{W_{lc} B_l + W_{mc} B_m}) = C \times \mathrm{e}^{i\theta B_l B_m} \tag{3.26}$$

for all the four possible values of the qubits values $B_l, B_m = \{0, 1\}$ and where C is an arbitrary (finite) normalization. A possible solution for this system is:

$$W_{lc} = -2\mathrm{A}(\theta) \tag{3.27}$$

$$W_{mc} = 2\mathrm{A}(\theta) \tag{3.28}$$

$$\Delta a_l = i\frac{\theta}{2} + \mathrm{A}(\theta) \tag{3.29}$$

$$\Delta a_m = i\frac{\theta}{2} - \mathrm{A}(\theta) \tag{3.30}$$

where $\mathrm{A}(\theta) = arccosh(\mathrm{e}^{-i\frac{\theta}{2}})$. Modifying the RBM's parameters accordingly will apply a CZ gate to its current state.

Pauli X gate

The X gate just flips the qubit l and the RBM amplitudes are:
$\langle \boldsymbol{v} \mid X_l \mid \psi_W \rangle = \langle v_1 \dots \bar{v_l} \dots v_N \mid \psi_W \rangle$.
Since $\bar{v_l} = (1 - v_l)$, it must be satisfied that

$$(1 - v_l) W_{lk} + b_k = v_l W_{lk}\prime + b_k\prime \tag{3.31}$$

and

$$(1 - B_l) a_l = B_l a_l\prime + C \tag{3.32}$$

hold for all the (two) possible values of $B_l = \{0, 1\}$. The solution to these equations is:

$$W_{lk}\prime = -W_{lk} \tag{3.33}$$

$$b_k\prime = b_k + W_{lk} \tag{3.34}$$

$$a_l\prime = -a_l \tag{3.35}$$

$$C = a_l, \tag{3.36}$$

whereas all the a_j and the other weights W_{jk} with $j \neq i$ are unchanged.

Pauli Y gate

A similar solution is also found for the Y gate, with the noticeable addition of extra phases with respect to the X gate:

$$W_{lk}\prime = -W_{lk} \tag{3.37}$$

$$b_k\prime = b_k + W_{lk} \tag{3.38}$$

$$a_l\prime = -a_l + i\pi \tag{3.39}$$

$$C = a_l + \frac{i\pi}{2}, \tag{3.40}$$

whereas all the a_j and other weights W_{jk} with $j \neq l$ are unchanged.

Pauli Z gate

The Pauli Z gate is a special case of the Z rotation with $\theta = \pi$. Thus the only change necessary is to set the bias a_l of the visible neuron l to

$$a_l\prime = a_l + i\pi. \tag{3.41}$$

3.5.2 Non-diagonal Gates

Exact applications of non-diagonal gates to Boltzmann machine quantum states would require introducing a second hidden layer [6]. In contrast to an RBM with just one hidden layer, this would make the calculation of the represented quantum state inefficient.

Thus, there are no rules for applying non-diagonal gates to an RBM state similar to those for diagonal gates. Nevertheless, the parameters of the RBM can be adapted in a supervised learning process instead.

The training set consists of samples drawn from the RBM with its current set of parameters. In the sampling process, the RBM's energy function can be adapted to resemble the energy states after a non-diagonal unitary gate G has been applied to its state.

For any non-diagonal unitary gate

$$G = \begin{pmatrix} a & b \\ c & d \end{pmatrix} \tag{3.42}$$

applied to qubit l, samples from the state $|\phi(\boldsymbol{v})\rangle = G_l\,|\psi(\boldsymbol{v})\rangle$ can be drawn according to

$$|\,|\phi(\boldsymbol{v}_{v_l=0})\rangle\,|^2 = |a\cdot|\psi(\boldsymbol{v}_{v_l=0})\rangle + c\cdot|\psi(\tilde{\approx}_{\tilde{\approx}_l=1})\rangle|^2 \tag{3.43}$$

when the state of qubit l is sampled to be 0 and

$$||\phi(\boldsymbol{v}_{v_l=1})\rangle|^2 = |b\cdot|\psi(\boldsymbol{v}_{v_l=0})\rangle + d\cdot|\psi(\boldsymbol{v}_{v_l=1})\rangle|^2. \tag{3.44}$$

when the state is sampled to be 1. This way, the samples are drawn with respect to their probabilities given by $||\phi\rangle|^2$.

Afterward, the samples are used to minimize the log-likelihood $L(\mathcal{W})$ of the overlap of the two quantum states ψ and ϕ, given by:

$$\begin{aligned} L(\mathcal{W}) &= -\log O(\mathcal{W}) && (3.45)\\ &= -\log\sqrt{\frac{|\langle\psi_{\mathcal{W}}\,|\,\phi\rangle|^2}{\langle\psi_{\mathcal{W}}\,|\,\psi_{\mathcal{W}}\rangle\,\langle\phi\,|\,\phi\rangle}} && (3.46)\\ &= -\log\sqrt{\left\langle\frac{\phi(\boldsymbol{v})}{\psi_{\mathcal{W}}(\boldsymbol{v})}\right\rangle_{\psi}\left\langle\frac{\psi_{\mathcal{W}}(\boldsymbol{v})}{\phi(\boldsymbol{v})}\right\rangle_{\phi}^{*}} && (3.47)\end{aligned}$$

with

$$\langle F(\boldsymbol{v})\rangle_A := \frac{\sum_{\boldsymbol{v}} F(\boldsymbol{v})|A(\boldsymbol{v})|^2}{\sum_{\boldsymbol{v}}|A(\boldsymbol{v})|^2} \tag{3.48}$$

with some gradient descent method. For Boltzmann machines, the gradients $\frac{\partial L}{\partial\theta_i} = \partial_{p_i}L(\mathcal{W})$ are of the form:

$$\partial_{p_i}L(\mathcal{W}) = \langle\mathcal{O}_k^*(\boldsymbol{v})\rangle_\psi - \frac{\langle\frac{\phi(\boldsymbol{v})}{\psi(\boldsymbol{v})}\mathcal{O}_k^*(\boldsymbol{v})\rangle_\psi}{\langle\frac{\phi(\boldsymbol{v})}{\psi(\boldsymbol{v})}\rangle_\psi}, \tag{3.49}$$

with $\mathcal{O}_k(\boldsymbol{v}) = \partial_{p_k}\log\psi_{\mathcal{W}}(\boldsymbol{v})$ being the variational derivatives of the RBMs wave function with respect to its parameters. These are simple to compute, since

$$\partial_{a_i}\log\psi_{\mathcal{W}}(\boldsymbol{v}) = v_i \tag{3.50}$$

$$\partial_{b_i}\log\psi_{\mathcal{W}}(\boldsymbol{v}) = h_i \tag{3.51}$$

$$\partial_{W_{ij}}\log\psi_{\mathcal{W}}(\boldsymbol{v}) = v_i h_j. \tag{3.52}$$

The quantum state $\psi_{\mathcal{W}}$, represented by the RBM, approximates the target state ϕ.

In summary, the procedure to apply non-diagonal quantum gates to a quantum state $|\psi(\mathcal{W})\rangle$ represented by an RBM is as follows:

1. Draw samples $\boldsymbol{d}_i = (\boldsymbol{c}_i, t_i)$ with Gibbs sampling and transition probabilities given by equation 3.43 and 3.44.
2. Calculate the gradients $\frac{\partial L}{\partial \theta_i}$ of the loss function defined in equation 3.49.
3. Use a gradient descent method like AdaMax or SR to update the parameters $\theta_i \in \mathcal{W}$.

This process is repeated for a predefined number of iterations. Using this approach and AdaMax as the optimization method, Jónsson et al. reported a per gate error of 10^{-3} [21].

Bibliography

[1] David H. Ackley, Geoffrey E. Hinton, and Terrence J. Sejnowski. A learning algorithm for boltzmann machines*. *Cognitive Science*, 9(1):147–169, 1985.

[2] Frank Arute, Kunal Arya, Ryan Babbush, Dave Bacon, Joseph Bardin, Rami Barends, Rupak Biswas, Sergio Boixo, Fernando Brandao, David Buell, Brian Burkett, Yu Chen, Jimmy Chen, Ben Chiaro, Roberto Collins, William Courtney, Andrew Dunsworth, Edward Farhi, Brooks Foxen, Austin Fowler, Craig Michael Gidney, Marissa Giustina, Rob Graff, Keith Guerin, Steve Habegger, Matthew Harrigan, Michael Hartmann, Alan Ho, Markus Rudolf Hoffmann, Trent Huang, Travis Humble, Sergei Isakov, Evan Jeffrey, Zhang Jiang, Dvir Kafri, Kostyantyn Kechedzhi, Julian Kelly, Paul Klimov, Sergey Knysh, Alexander Korotkov, Fedor Kostritsa, Dave Landhuis, Mike Lindmark, Erik Lucero, Dmitry Lyakh, Salvatore Mandrà, Jarrod Ryan McClean, Matthew McEwen, Anthony Megrant, Xiao Mi, Kristel Michielsen, Masoud Mohseni, Josh Mutus, Ofer Naaman, Matthew Neeley, Charles Neill, Murphy Yuezhen Niu, Eric Ostby, Andre Petukhov, John Platt, Chris Quintana, Eleanor G. Rieffel, Pedram Roushan, Nicholas Rubin, Daniel Sank, Kevin J. Satzinger, Vadim Smelyanskiy, Kevin Jeffery Sung, Matt Trevithick, Amit Vainsencher, Benjamin Villalonga, Ted White, Z. Jamie Yao, Ping Yeh, Adam Zalcman, Hartmut Neven, and John Martinis. Quantum supremacy using a programmable superconducting processor. *Nature*, 574:505–510, 2019.

[3] Yoshua Bengio. Rmsprop and equilibrated adaptive learning rates for non-convex optimization. *corr abs/1502.04390*, 2015.

[4] Yoshua Bengio et al. Learning deep architectures for ai. *Foundations and trends® in Machine Learning*, 2(1):1–127, 2009.

[5] Ethan Bernstein and Umesh Vazirani. Quantum complexity theory. In *in Proc. 25th Annual ACM Symposium on Theory of Computing, ACM*, pages 11–20, 1993.

[6] Giuseppe Carleo, Yusuke Nomura, and Masatoshi Imada. Constructing exact representations of quantum many-body systems with deep neural networks. *Nature communications*, 9(1):1–11, 2018.

[7] Giuseppe Carleo and Matthias Troyer. Solving the quantum many-body problem with artificial neural networks. *Science*, 355(6325):602–606, 2017.

[8] Dong-Ling Deng, Xiaopeng Li, and S Das Sarma. Quantum entanglement in neural network states. *Physical Review X*, 7(2):021021, 2017.

[9] Guillaume Desjardins, Aaron Courville, Yoshua Bengio, Pascal Vincent, and Olivier Delalleau. Parallel tempering for training of restricted boltzmann machines. In *Proceedings of the thirteenth international conference on artificial intelligence and statistics*, pages 145–152. MIT Press Cambridge, MA, 2010.

[10] John Duchi, Elad Hazan, and Yoram Singer. Adaptive subgradient methods for online learning and stochastic optimization. *Journal of machine learning research*, 12(Jul):2121–2159, 2011.

[11] Richard P Feynman. Simulating physics with computers. *Int. J. Theor. Phys*, 21(6/7), 1982.

[12] Asja Fischer and Christian Igel. An introduction to restricted boltzmann machines. pages 14–36, 01 2012.

[13] Josiah Willard Gibbs. *Elementary Principles in Statistical Mechanics: Developed with Especial Reference to the Rational Foundation of Thermodynamics*. Cambridge Library Collection - Mathematics. Cambridge University Press, 2010.

[14] John Gill. Computational complexity of probabilistic turing machines. *SIAM Journal on Computing*, 6(4):675–695, 1977.

[15] Daniel Gottesman. The heisenberg representation of quantum computers, 1998.

[16] W Keith Hastings. Monte carlo sampling methods using markov chains and their applications. 1970.

[17] Geoffrey Hinton. *Boltzmann Machines*, pages 132–136. Springer US, Boston, MA, 2010.

[18] Geoffrey E Hinton. Training products of experts by minimizing contrastive divergence. *Neural computation*, 14(8):1771–1800, 2002.

[19] Geoffrey E Hinton, Simon Osindero, and Yee-Whye Teh. A fast learning algorithm for deep belief nets. *Neural computation*, 18(7):1527–1554, 2006.

[20] Geoffrey E. Hinton and Terrence J. Sejnowski. Analyzing cooperative computation. In *Proceedings of the Fifth Annual Conference of the Cognitive Science Society, Rochester NY*, 1983.

[21] Bjarni Jónsson, Bela Bauer, and Giuseppe Carleo. Neural-network states for the classical simulation of quantum computing, 2018.

[22] Diederik P Kingma and Jimmy Ba. Adam: A method for stochastic optimization. *arXiv preprint arXiv:1412.6980*, 2014.

[23] A.Y. Kitaev, A. Shen, M.N. Vyalyi, and M.N. Vyalyi. *Classical and Quantum Computation*. Graduate studies in mathematics. American Mathematical Society, 2002.

[24] Nicolas Le Roux and Yoshua Bengio. Representational power of restricted boltzmann machines and deep belief networks. *Neural computation*, 20(6):1631–1649, 2008.

[25] Guido Montufar. Restricted boltzmann machines: Introduction and review, 2018.

[26] Guido Montufar and Nihat Ay. Refinements of universal approximation results for deep belief networks and restricted boltzmann machines. *Neural computation*, 23(5):1306–1319, 2011.

[27] Michael A Nielsen and Isaac Chuang. Quantum computation and quantum information, 2002.

[28] John Preskill. Quantum computing and the entanglement frontier, 2012.

[29] Sebastian Ruder. An overview of gradient descent optimization algorithms., 2016. cite arxiv:1609.04747Comment: Added derivations of AdaMax and Nadam.

[30] John E. Savage. *Models of Computation: Exploring the Power of Computing*. Addison-Wesley Longman Publishing Co., Inc., USA, 1st edition, 1997.

[31] Henry Maurice Sheffer. A set of five independent postulates for boolean algebras, with application to logical constants. *Transactions of the American Mathematical Society*, 14(4):481–488, 1913.

[32] Peter W. Shor. Polynomial-time algorithms for prime factorization and discrete logarithms on a quantum computer. *SIAM Journal on Computing*, 26(5):1484–1509, Oct 1997.

[33] Paul Smolensky. Information processing in dynamical systems: Foundations of harmony theory. Technical report, Colorado Univ at Boulder Dept of Computer Science, 1986.

[34] S. Sorella. Green function monte carlo with stochastic reconfiguration, 1998.

[35] Tijmen Tieleman. Training restricted boltzmann machines using approximations to the likelihood gradient. In *Proceedings of the 25th international conference on Machine learning*, pages 1064–1071, 2008.

[36] A. M. Turing. On Computable Numbers, with an Application to the Entscheidungsproblem. *Proceedings of the London Mathematical Society*, s2-42(1):230–265, 01 1937.